A Robust Control Approach for Frequency Support Capability of Grid-Tie Photovoltaic Systems

Sid Ahmed El Mehdi Ardjoun, first author[1]
IRECOM Laboratory, Faculty of Electrical Engineering, Djillali Liabes University
22000 Sidi Bel-Abbes, Algeria
elmehdi.ardjoun@univ-sba.dz

Mouloud Denaï, second author
School of Physics, Engineering and Computer Science, University of Hertfordshire,
Hatfield, United Kingdom
m.denai@herts.ac.uk

Houcine Chafouk, third author
Normandy University, UNIROUEN, ESIGELEC, IRSEEM,
76000 Rouen France
houcine.chafouk@esigelec.fr

ABSTRACT

Distributed solar Photovoltaic (PV) generation is growing rapidly around the world. However, unlike conventional synchronous generators, PV systems do not have any rotating masses to deliver inertia to support the grid frequency. The paper presents a detailed modeling of a new converter configuration and control scheme to enable PV systems to adjust the real power output and contribute to the grid frequency regulation. The proposed topology consists of a two-stage converter without an energy storage system. A dc-dc buck converter is used instead of a dc-dc boost converter, and this simplifies the control scheme which aims to keep the PV generator power in the right side of the P-V characteristic and can be varied in the range from near-zero to the maximum power. The proposed control scheme combines robust and nonlinear sliding mode theory with fuzzy logic. The PV system is connected to a low inertia microgrid and its ability to contribute to frequency regulation is assessed for different controls. The proposed converter and its control

[1] Corresponding author Sid Ahmed El Mehdi Ardjoun.

are validated experimentally on a 3-kW PV system using OPAL-RT real-time simulator and tested under varying temperature, solar irradiance, and partial shading conditions. The results show that with the proposed circuit, the operating point is always on the right side of the P-V characteristic irrespective of the operating mode. Furthermore, the proposed control scheme provides PV generators with a fast and effective inertial response to support the grid and enhance its stability during contingencies.

Keywords: grid frequency regulation, inertial response, photovoltaic systems, partial shading, real power control, fuzzy logic, sliding mode control.

1. INTRODUCTION

The energy sector across the world is undergoing a profound transition from carbon-intensive energy to low-carbon, renewable energy. This transformation is due to the excessive exploitation of fossil fuels over the past decades which has generated collateral effects causing global warming of the planet and a rapid decline in the reserves of these natural resources. Among these renewable sources, solar energy is one of the most abundant and will remain the ultimate energy source across all parts of the world.

In recent years, photovoltaic (PV) technology has been the most prominent technique for electricity generation and has an enormous potential to address the global future energy challenges [1]. According to the International Renewable Energy Agency (IRENA), grid-tied PV capacity reached 843.086 GW and off-grid reached 4.865 GW in 2021 [2]. The significant increase in PV installed capacity is mainly due to technological improvements and government policies to introduce feed-in tariffs, rebates, and incentives to promote the adoption of the PV systems in homes and businesses which have considerably reduced their costs [3].

Therefore, the gradual replacement of conventional generators with PV distributed generation will reduce the system's inertia and increase the sensitivity of the grid frequency during power imbalance [4]. To overcome such a problem and ensure the security of the electricity grid, many countries have revised their technical regulations for connecting distributed generation sources to the electricity grid [5]. As a result, PV systems are now required to participate in frequency regulation to enhance grid security [6].

In this context, two approaches have been adopted. The indirect approach uses a storage system; the PV generators (PVG) indirectly participate in the frequency regulation. However, the indirect approach generally involves a high investment cost to deploy the grid-scale energy storage facility [7]. The direct approach, on the other hand, consists in modifying the control of the PVG to reduce their output power below the maximum power. Thus, an amount of real power is reserved, and can be injected into the grid in the event of frequency drop. Alternatively, if there is an increase in frequency, the real power must be reduced. The direct method has been investigated by several researchers, and the feasibility of this technique has been demonstrated on a 300 MW PV power plant in California [8]. The successful implementation of such a technique requires (i) accurate real-time estimation of the available power of the PVGs, (ii) rapid and effective response of the controlled real power [8].

Concerning the area related to rapid and effective real power response of PVGs, it is a relatively new area of research, and very little work has been done. Rapid response of the real power is useful in stabilizing the frequency, especially in a low inertia grid [9]. The real power response must be less than one second (for example 0.5 sec [10] or 0.1 sec [11]), depending on the grid code. But it should be noted that with classical control methods, the PVG power response is slow (greater than 1 sec) [8]. Recent research has focused on improving the real power response of PVGs. As an example, in [12] the authors have investigated a PV-STATCOM smart inverter and have shown the need for a rapid response of the real power to achieve a fast frequency response. The control proposed by these authors is based on PI controllers tuned with a systematic trial and error approach. In [9], the authors proposed a predictive control of the dc-ac converter to ensure a very fast and accurate control of the real power. But they pointed out that the proposed method required irradiance and temperature measurements, which would increase the cost of the system. In addition, this method produced transient and steady-state errors and therefore is not sufficiently accurate.

The authors in [9] and [12] used the same converter topology (single-stage inverters), but the range of the DC output voltage of this converter type is limited [13]. So the range of PVG power variability will be limited, and its capacity to participate in the grid frequency regulation will also be limited. To achieve a wider range (from near zero to maximum power), the authors in [14] used a two-stage configuration based on a dc-dc converter and a dc-ac converter. This configuration provides flexible operation and the control of PV systems, because the DC link voltage of the PV inverter is decoupled from the PVG voltage [15]. The two-stage configuration is widely used in large-scale grid-tie PV systems [16]. Thus the dc-dc converter control needs to be changed to control the PVG power. However, from the control perspective, it will make the PVG participation in the grid frequency regulation more difficult [17]. Because the P-V characteristic of a PVG is non-monotonic, therefore, it is recommended that the operating point is varied in the right side of the PVG characteristic in order to have a good performance of the PVG (this will be discussed in Section 4).

Several authors have tried to address the problem of keeping the operating point in the right side of the PVG characteristic. In [18], the authors proposed to vary the PVG power by a dc-dc boost converter and a PI controller to regulate the PVG output voltage. However, they could not achieve a precise power tracking. So, in [17] the authors proposed to add another PI controller to control both power and voltage. But the suggested solution requires the use of three controllers, for the frequency, power and voltage which need to be tuned properly to achieve the desired stability. In addition, the authors did not show how to avoid the left side of the PV characteristic.

On the other hand, in [19] the authors proposed to use only a PI controller to control the PVG power instead of controlling its voltage. But a single controller is insufficient to keep the operating point in the right side of the PV characteristic. So, in [14] the authors proposed to add an algorithm to the controller. The principle of this algorithm is that the PI controller considers a modified version of the PV characteristic, instead of the actual characteristic. The modified characteristic reflects the left side of the PV characteristic as a horizontal line passing through the MPP (maximum power point). So, if the operating point is located on the left side of the characteristic, then a negative error results, which shifts the operating point to the right side of the characteristic. However, this technique is faulty during partial shading. So, in [20], the authors propose to improve the algorithm, but this has increased the complexity of the control. Because under partial shading conditions, the P-V characteristic becomes more complex which makes proper modification quite difficult.

To address the limitations of the above methods, our paper proposes to replace the dc-dc boost converter with a dc-dc buck converter. The buck converter requires a simple control of the PVG to operate only in the right side of its characteristic in the range from near-zero to the maximum power. This will increase the PVG capacity to participate in the grid frequency regulation. Furthermore, a robust Fuzzy Sliding Mode (FSM) controller is designed to control the PV power.

The remaining of the paper is organized as follows: Section 2 describes the PV energy conversion system connected to the power grid. Section 3 represents the technical issues of the grid code on the management of real power relating to frequency regulation. Section 4 and 5 present in detail the proposed buck converter topology and its control strategy respectively. Finally, the simulation results using OPAL-RT real-time simulator and the conclusion are presented in Sections 6 and 7 respectively.

2. Description of the PV System Connected to the Electricity Grid

The PV energy conversion system studied is based on two converters: dc/dc and dc/ac as shown in Fig. 1. This configuration is widely used in large-scale grid-tie PV systems [16].

The single diode model of the PVG is described by the following equation [21]:

$$I_{pv} = N_p I_{sc} - N_p I_{sat}\left[\exp\left(\frac{1}{nV_t}\left(\frac{V_{pv}}{N_s}+\frac{I_{pv}R_s}{N_p}\right)\right)-1\right]-\frac{N_p}{R_p}\left(\frac{V_{pv}}{N_s}+\frac{I_{pv}R_s}{N_p}\right) \tag{1}$$

Where $V_t = KT/e$

The buck converter consists of a MOSFET which is connected to an anti-parallel diode. The inverter consists of three switching cells, each made up of two IGBT transistors connected to two anti-parallel diodes to provide bidirectional current flow. In this study, all switches are assumed ideal and therefore switching losses are neglected. Filters are employed to eliminate the harmonics generated by the converters. Since a dc/dc buck converter is used, a transformer is required for the connection to the grid. The transformer allows, on the one hand, to raise the voltage supplied by the inverter to the desired value required by the grid, and on the other hand to provide galvanic isolation between the two energy sources. In this study, a three-phase Delta-Star connected 180 V /380 V transformer is used.

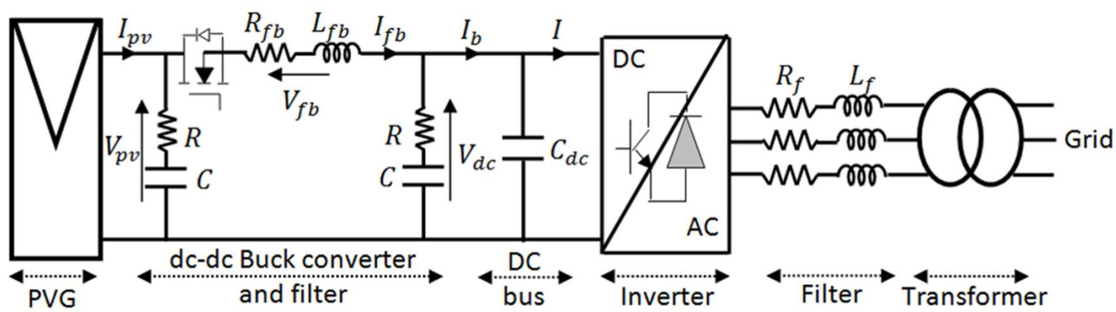

Figure 1. Grid connected PV energy conversion system

3. Grid Code Technical Issues on Real Power Management

Currently, distributed PV generation is increasingly being called upon to comply with the requirements imposed by the grid operator. Among these requirements are the real power control modes relating to frequency regulation. In the Danish grid code [6], for example, there are different types of real power controls to connect PV plants to the grid. These modes can be requested by the grid manager based on the system status and operating conditions. There are five technical issues which are briefly summarized in the Appendix 1.

4. Proposed Solution to Operate PVGs at Variable Powers

This section presents the solution proposed to enable PVGs to operate with variable power and comply with the technical requirements imposed by the grid codes.

In Figure. 2 are shown typical I-V and P-V characteristics of a PVG for a given temperature and irradiation. To control the PVG power over the entire range from near-zero to the maximum power (P_{ref} dotted lines), the PVG output voltage V_{pv} must be varied. Hence there are several possible operating points located on each side of the MPP: the left operating points (circle marker) and the right operating points (lozenge marker). However, two of these operating points (open circuit voltage V_{oc} and short circuit current I_{sc}) must be avoided in order not to damage the PVG [22]. Clearly, the operation of the PVG in the right side of the MPP (high voltage) is relatively better than in the left side (low voltage). This is due to several reasons: to avoid the high current which heats the PVG reducing its efficiency, and to have a faster dynamic response, since on the right side, the slope of the characteristic P-V is steeper than on the left side [14].

If the voltage of GPV is controlled by a dc-dc boost, and there are rapid changes in irradiance and temperature, the operating point may be shifted to the left side despite the working point is on the right side [14]. Thus, the proposed solution consists of using a buck converter because it does not require an additional complex algorithm to the PVG control and it ensures that the PV system always operates on the right side of the characteristic under any operating conditions.

In fact, static converters connected to the grid generally operate at a constant DC bus voltage (V_{dc}) in order to have a better power flow. The duty cycle of the dc-dc converter is adjusted to vary the input voltage of the converter (V_{pv}). Since a buck converter is employed, then the input voltage value (V_{pv}) is always greater than or equal to the output voltage value (V_{dc}). Furthermore, to ensure that the PVG always operates in the right side of the MPP, the V_{dc}value must be kept equal or very close to the optimal value V_{opt} of the PVG.

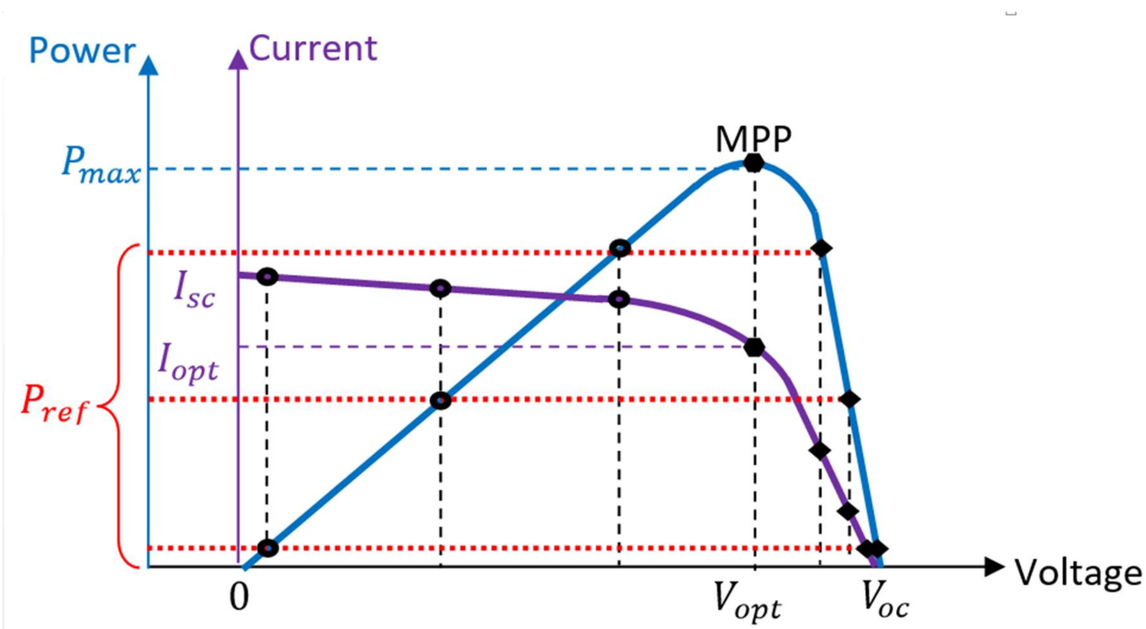

Figure 2. PVG I-V and P-V characteristics

5. Control Scheme of the Grid-Tie PV Power System

With reference to Fig.1, two control schemes are therefore necessary to ensure the operation of the system: (i) control of the buck converter to regulate the power produced by the PVG, (ii) control of the inverter via the regulation of the DC bus voltage and the real and reactive powers exchanged with the grid (the inverter control is detailed in the Appendix 2).

5.1. Overview of PV power control using classical PI regulator

To control the power produced by the PVG, it is necessary to control the output voltage V_{pv} of the PVG according to the desired reference power. This is achieved by adjusting the duty cycle α of the buck converter and by controlling the filter current I_{fb}.

To derive the control law, we use the equations of the buck converter and its filter [23].

When the switch is closed ($0 < t < \alpha T_s$):

$$V_{pv} = R_{fb} I_{fb} + L_{fb} \frac{dI_{fb}}{dt} + V_{dc} \tag{2}$$

$$\frac{dI_{fb}}{dt} = \frac{1}{L_{fb}} \left(V_{pv} - V_{dc} - R_{fb} I_{fb} \right) \tag{3}$$

When the switch is open ($\alpha T_s < t < T_s$):

$$0 = R_{fb} I_{fb} + L_{fb} \frac{dI_{fb}}{dt} + V_{dc} \tag{4}$$

$$\frac{dI_{fb}}{dt} = -\frac{1}{L_{fb}} \left(V_{dc} + R_{fb} I_{fb} \right) \tag{5}$$

Equations (3) and (5) describe the dynamics of the current in the filter ($R_{fb} L_{fb}$) of the buck converter for the periods αT_s and $(1-\alpha) T_s$ respectively. To find an approximate dynamic representation that is valid for both time intervals, it will be assumed that the current I_{fb} has a linear form, hence its derivative will be constant.

Based on this assumption, the expression of the mean value of the current can be decomposed over the two time periods αT_s and$(1-\alpha)T_s$:

$$\frac{dI_{fb}}{dt}.T_s = \frac{dI_{fb}}{dt_{(dT_s)}}.\alpha T_s + \frac{dI_{fb}}{dt_{((1-d)T_s)}}.(1-\alpha)T_s \tag{6}$$

Substituting Eq. (3) and (5) in (6) yields the equation which governs the system over an entire period:

$$\frac{dI_{fb}}{dt} = \frac{1}{L_{fb}}\left(\alpha V_{pv} - V_{dc} - R_{fb}I_{fb}\right) \tag{7}$$

Thus, the control law can be deduced as:

$$\alpha = \frac{V_{fb} + V_{dc}}{V_{pv}} \tag{8}$$

The purpose of the control is to find the duty cycle α for each reference power value. Since in our system the voltage V_{dc} is set by the dc/ac converter, therefore by varying the duty cycle, the voltage V_{pv} as well as the power of the PVG can be varied. Based on Eq. (8), the duty cycle can be varied by changing the filter voltage V_{fb} which is, in turn, dependent on the current flowing through the filter (I_{fb}). So, from the reference power, the reference current $I_{fb_{ref}}$ can be calculated and to ensure continuous flow of the current during the power variation, a controller is required.

Figure 3.a shows the block diagram of the buck converter control.

The block diagram of the closed-loop control of the current I_{fb} is shown in Fig.3.b.

The PI controller parameters are calculated so that the closed-loop transfer function is first order with time-constant $t_s^{I_{fb}}$.

$$\begin{cases} K_p^{I_{fb}} = \dfrac{3L_{fb}}{t_s^{I_{fb}}} \\ K_i^{I_{fb}} = \dfrac{3R_{fb}}{t_s^{I_{fb}}} \end{cases} \tag{9}$$

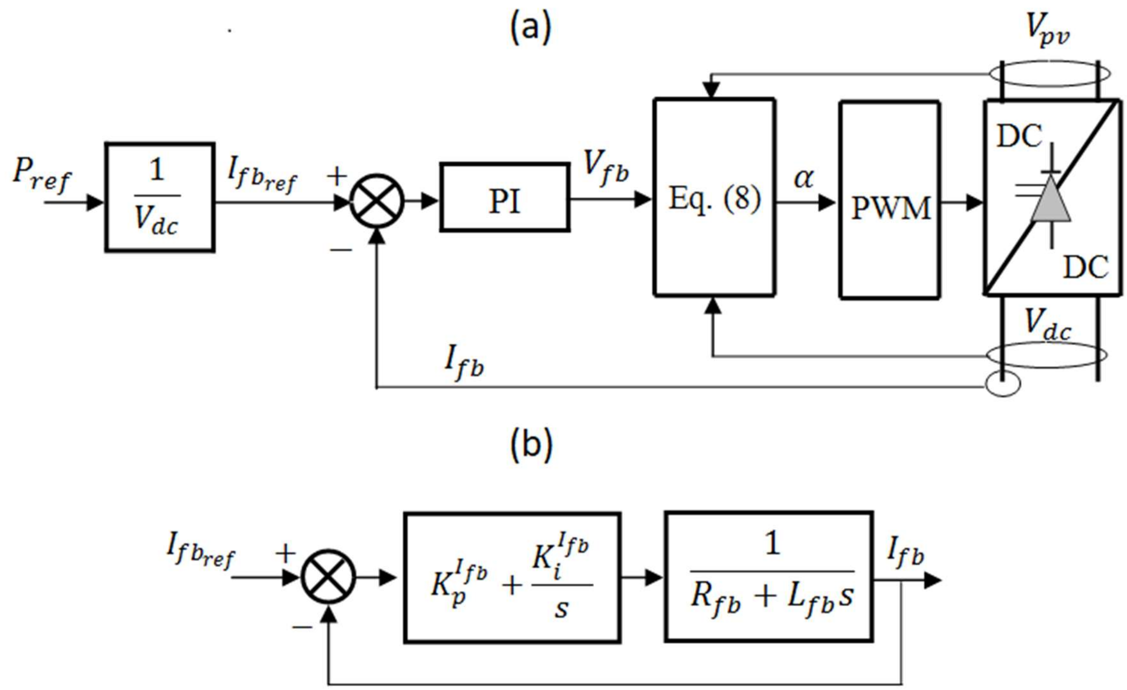

Figure 3. Classical control scheme of the buck converter: (a) general scheme, (b) I_{fb} current control block diagram

5.2. Robust fuzzy sliding mode control

Our paper proposes a hybrid control strategy combining the robust features of sliding mode and fuzzy logic controllers to overcome the limitations of classical PI controllers [24].

The sliding surface is defined as follows [25]:

$$S(X) = \left(\frac{d}{dt} + \lambda\right)^{n-1} e \tag{10}$$

Where n is the relative degree to the drift number, and λ is a positive constant.

Let e be the error of the chopper filter current, and if we set n = 1, then the expression of the surface has the form:

$$S(I_{fb}) = I_{fb_{ref}} - I_{fb} \tag{11}$$

The control law can be defined as:

$$V_{fb} = V_{fb}^{eq} + V_{fb}^{fuzzy} \tag{12}$$

Where the filter voltage V_{fb} is chosen as the control vector which consists of two control terms. The first term (V_{fb}^{eq}), called equivalent control, maintains the state of the system on the surface, and the second term (V_{fb}^{fuzzy}) is the fuzzy controller which forces the trajectory of the system to converge on the surface. The latter has the advantage of eliminating the chattering effect.

By taking the derivative of the surface and substituting the expressions of the filter current derivative and V_{fb}, gives:

$$\dot{S}(I_{fb}) = \dot{I}_{fb_{ref}} - \frac{1}{L_{fb}}\left[\left(V_{fb}^{eq} + V_{fb}^{fuzzy}\right) - R_{fb}I_{fb}\right] \tag{13}$$

During the sliding mode, we have: $S(I_{fb}) = 0, \dot{S}(I_{fb}) = 0,\ V_{fb}^{fuzzy} = 0$. Hence, the expression of the equivalent control is written:

$$V_{fb}^{eq} = L_{fb}\dot{I}_{fb_{ref}} + R_{fb}I_{fb} \tag{14}$$

Substituting the expression of the equivalent control in Eq. (13), yields:

$$\dot{S}(I_{fb}) = -\frac{1}{L_{fb}}V_{fb}^{fuzzy} \tag{15}$$

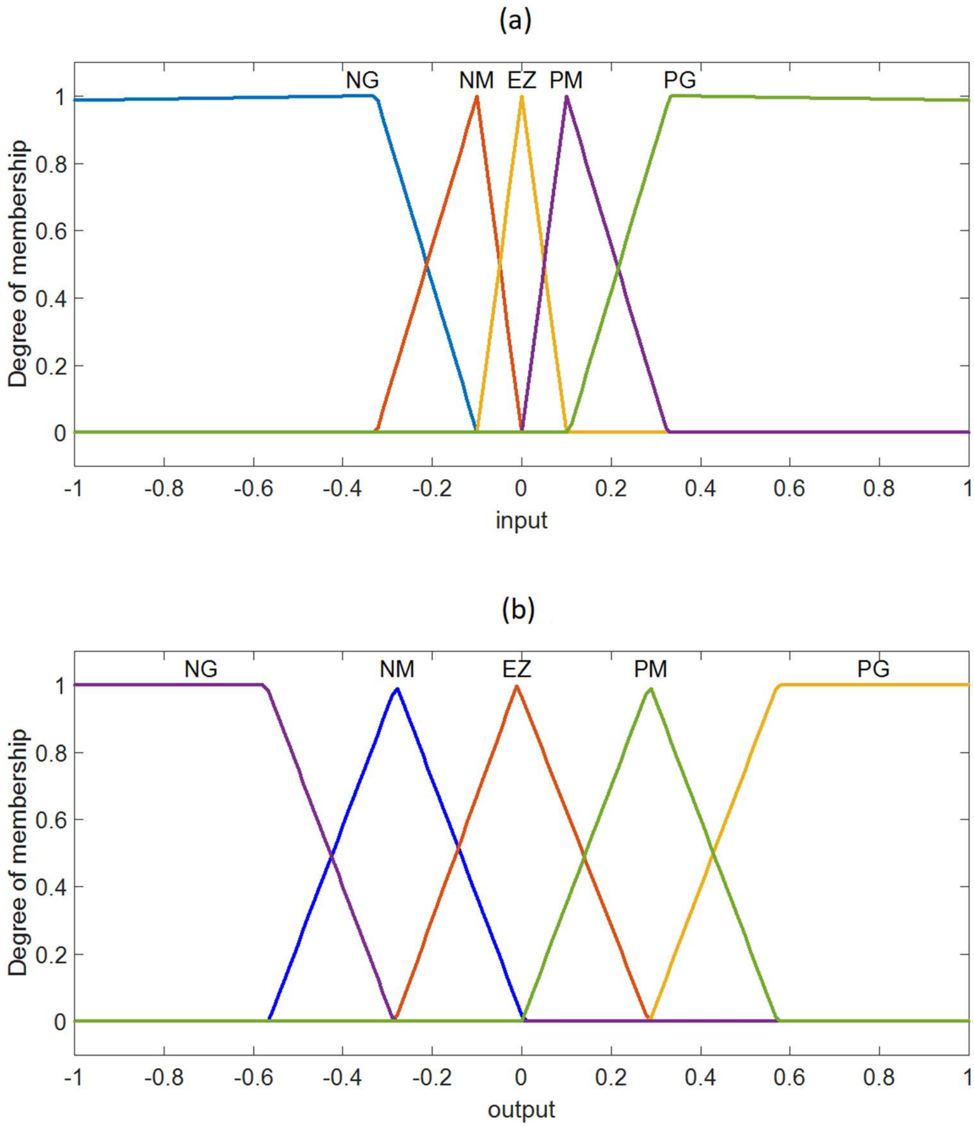

Figure 4. Membership functions: (a) input variables $S(I_{fb})$, (b) output variables V_{fb}^{fuzzy}

To ensure convergence towards the surface, the condition $S(I_{fb})\dot{S}(I_{fb}) \leq 0$ must hold. To achieve the convergence condition, the fuzzy sets, the membership functions and the fuzzy rules are defined as follows:

For the input variable $S(I_{fb})$ and for the output variable V_{fb}^{fuzzy}, the fuzzy sets are defined as: Positive Big (PB), Positive Medium (PM), Equal Zero (EZ), Negative

Medium (NM) and Negative Big (NB). The membership functions are depicted in Fig.4. Membership function aggregation and Mamdani's fuzzy inference are based on the max operator. The center of gravity defuzzification method is used for the control output. Thus the rules which ensure the convergence condition are presented in Table 1.

Table 1 Fuzzy rules

Rules	1	2	3	4	5
If $S(I_{fb})$ is	NB	NM	EZ	PM	PG
V_{fb}^{fuzzy} must be	NB	NM	EZ	PM	PG
Therefore according to the Eq. (15) $\dot{S}(I_{fb})$ is	PB	PM	EZ	NM	NG
Convergence condition	assured	assured	assured	assured	assured

Figure 5 shows the block diagram of the buck converter control with FSM.

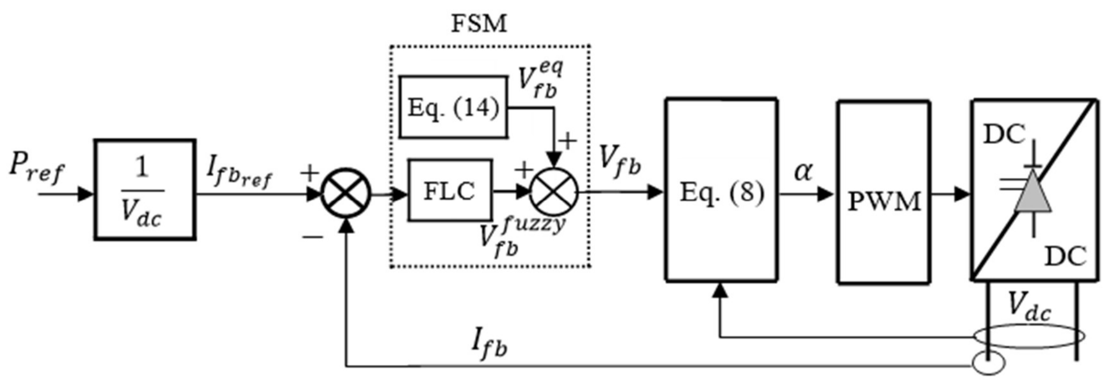

Figure 5. FSM control scheme of the buck converter

6. Simulation Results

To validate the converter configuration and its control scheme proposed, two different case scenarios of real time simulations are carried out under RT-LAB. The first scenario is aimed to assess the performance of the proposed PV system regardless of the power imposed by the grid manager. In the second scenario, the inertial frequency response of the proposed PV system is tested under load variations and partial shading.

6.1 Performance assessment of the PV system and control scheme

Table 2 PV system parameter values

Parameter	Value	Unit
P_{pv}	3	kW
N_s	360	
N_p	2	
I_{sc}	7	A
I_{sat}	4.3e-7	A
V_{oc}	230.4	V
V_t	0.0257	V
K	1.38e-23	J/°K
e	1.602e-19	C
n	1.5	
R_s	1e-03	Ω
R_p	1e-03	Ω
R	0.25	Ω
R_{bf}	0.1	Ω
R_f	1	Ω
L_{bf}	402e-6	H
L_f	2.5e-3	H
C	12e-4	F
C_{dc}	3.6	F
ω_s		rad/sec
θ_s		rad
t_s	0.1	sec
ξ	0.707	
ω_0	27	rad/sec

In the first study, a 3 kW PVG connected to an infinite bus electrical grid is considered. The parameters of the PVG are listed in Table 2. To assess the robustness of the control, the resistance R_{bf} was increased by 50%, and the inductance L_f was decreased by 50%.

The reference voltage of the DC bus is fixed at 180 V and the capacitors are initially charged at 180 V. The reference reactive power Q_{ref} is fixed at 0 VAR.

The first simulation test consists in imposing several reference power modes according to the grid code, then compare the results of the PI control to those of FSM control. The reference power modes are given as follows:

- Delta mode (Fig.7. Left panel): in this mode a reserve of 20% has been imposed ($P_{ref} = 0.8\ P_{max}$).
- Balance mode (Fig.7. Right panel): in this mode, $P_{ref} = 1\ KW$ has been imposed.

The system operation is simulated over a period of 24 hours, with varying temperature, irradiation (Fig.6).

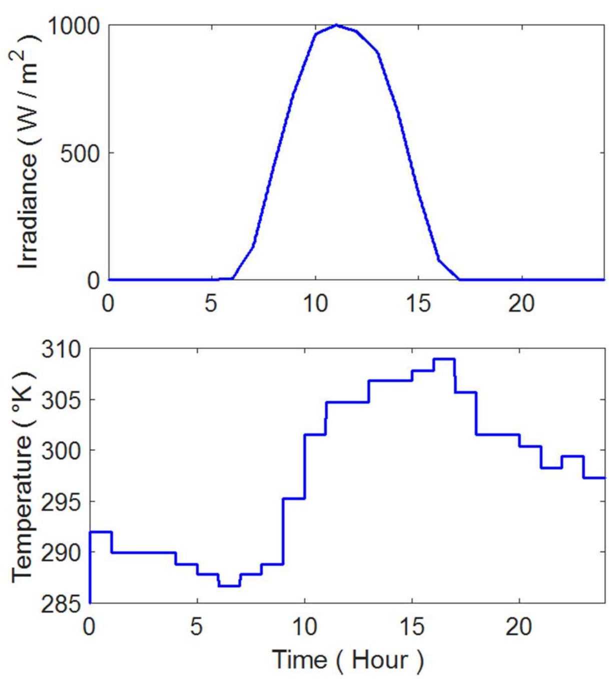

Figure 6. Solar irradiance and temperature profiles used in the model

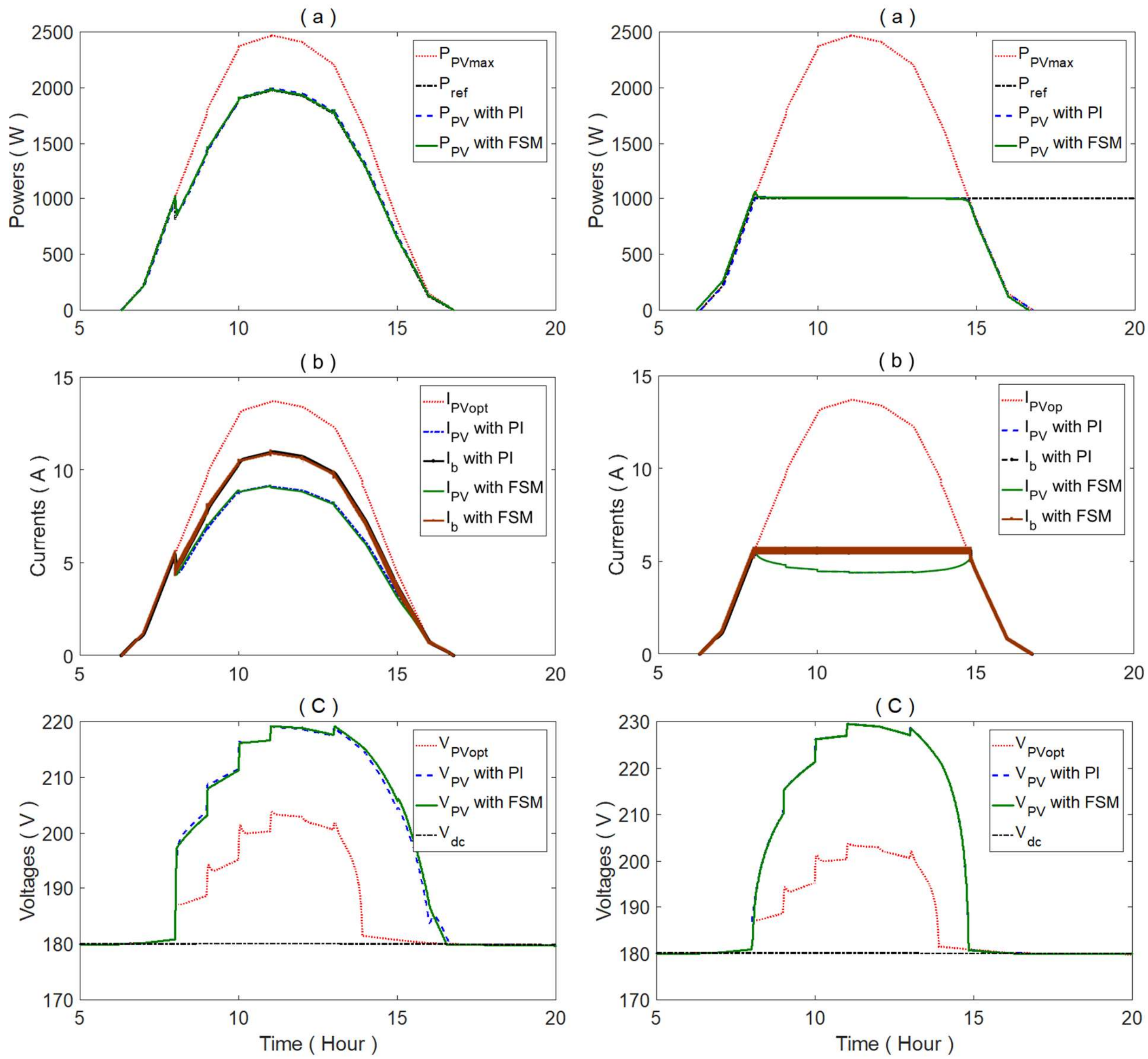

Figure 7. Left panel: Responses in delta mode. Right panel: Responses in balance mode: (a) powers, (b) currents, (c) voltage

From the results shown in Fig.7, the following conclusion can be drawn:

- A similarity between the responses obtained with the PI control and the FSM control.
- The power produced by the PVG perfectly follows its reference with a very small steady-state error, irrespective of which mode is being used (see Fig 7.a).

- The responses of the currents are similar to those of the powers (see Fig 7.a and Fig 7.b).
- The buck converter current (I_b) is always greater than the PV current (I_{pv}), and is always lower than the optimal PV current ($I_{pv_{opt}}$), see Fig 7.b. It confirms that the system is operating in the right side of the PVG characteristic.
- The voltage V_{dc} follows its reference and the voltage V_{pv} is variable due to the extraction of the desired power. In addition, the V_{pv}voltage is always higher than the voltages V_{dc} and $V_{pv_{opt}}$ (see Fig 7.c). Thus it also confirms that our system is operating in the right side of the PVG characteristic.

Thus, according to these results, it can be noted that despite the variation of the irradiation and temperature and regardless of the control mode, the proposed control system is operating in the right side of the PVG characteristic. It is also able to adapt quickly to the changing operating conditions and provides accurate regulation of the voltages and currents to deliver the desired power required by the grid.

6.2. Performance assessment for grid frequency regulation

In the second study, a low inertia microgrid with high penetration of PV sources is considered. As shown in Fig.8, the microgrid consists mainly of a DG diesel generator (a voltage source which imposes the amplitude and frequency of the microgrid voltage), the proposed PV system (a current source which imposes a power for a given voltage) and variable loads (P_L). The mathematical model of the system considered is shown in

Fig.8.b. All the parameter values of the model are expressed in p.u. The parameters of the microgrid are listed in Table 3.

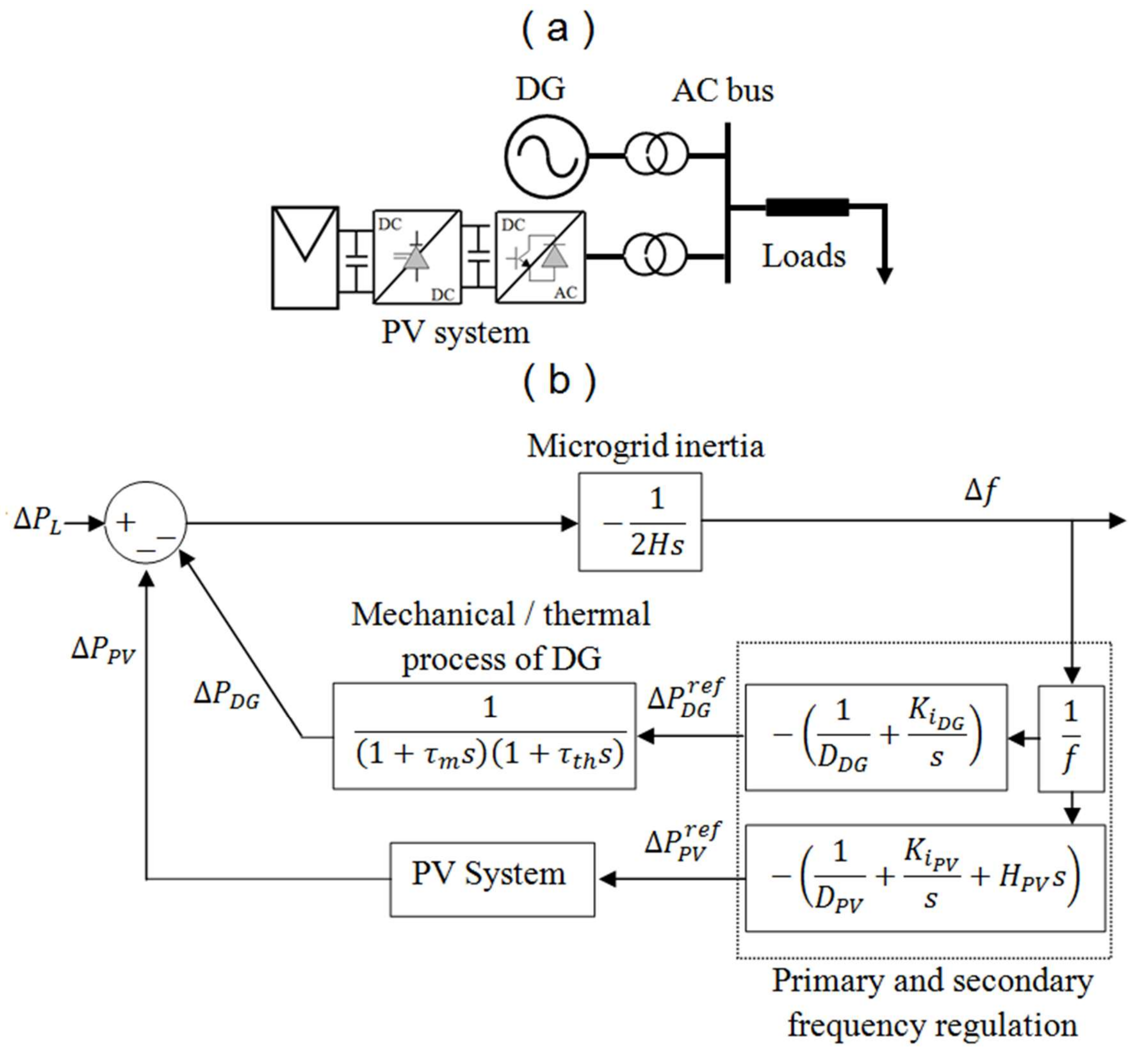

Figure 8. Low inertia microgrid: (a) configuration (b) transfer function bloc diagram

Table 3 Microgrid parameter values.

Parameter	Value	Unit
v_g	380	V
f	50	Hz
H	0.1	sec

H_{PV}	10	sec
$D_{PV} = D_{DG}$	5	%
$K_{i_{PV}} = K_{i_{DG}}$	20	sec^{-1}
τ_m	0.1	sec
τ_{th}	0.2	sec

The aim of the study is then to involve the PV system in the grid frequency regulation by delivering the required real power according to the frequency measured locally. So the PV system must be able to add synthetic inertia (H_{PV}), to perform droop control (D_{PV}) and also to participate in secondary regulation which requires the addition of an integral gain ($K_{i_{PV}}$). All these parameters will be adjusted one after the other to limit the frequency deviation to 0.4 Hz when a load of 0.8 p.u. is used. Then imposing two different depth of a partial shading that will affect half of the PVG (Fig.9).

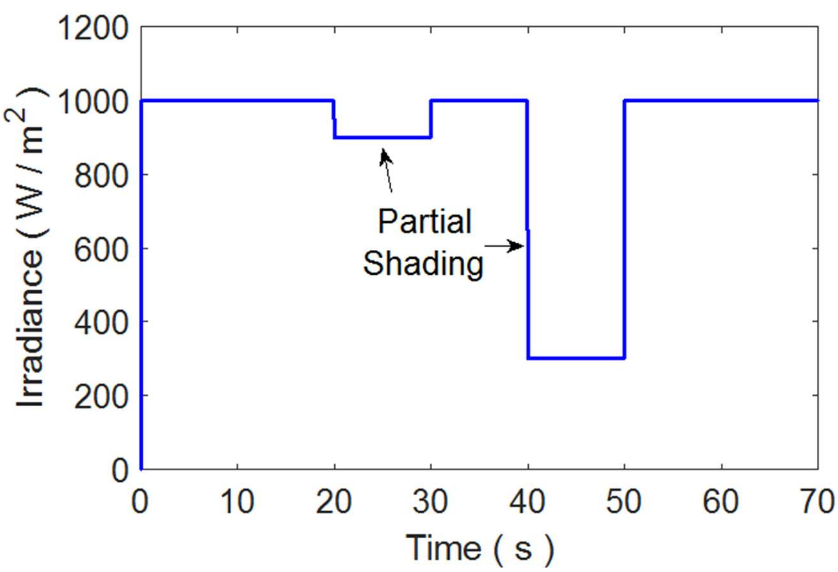

Figure 9. Partial shading profiles

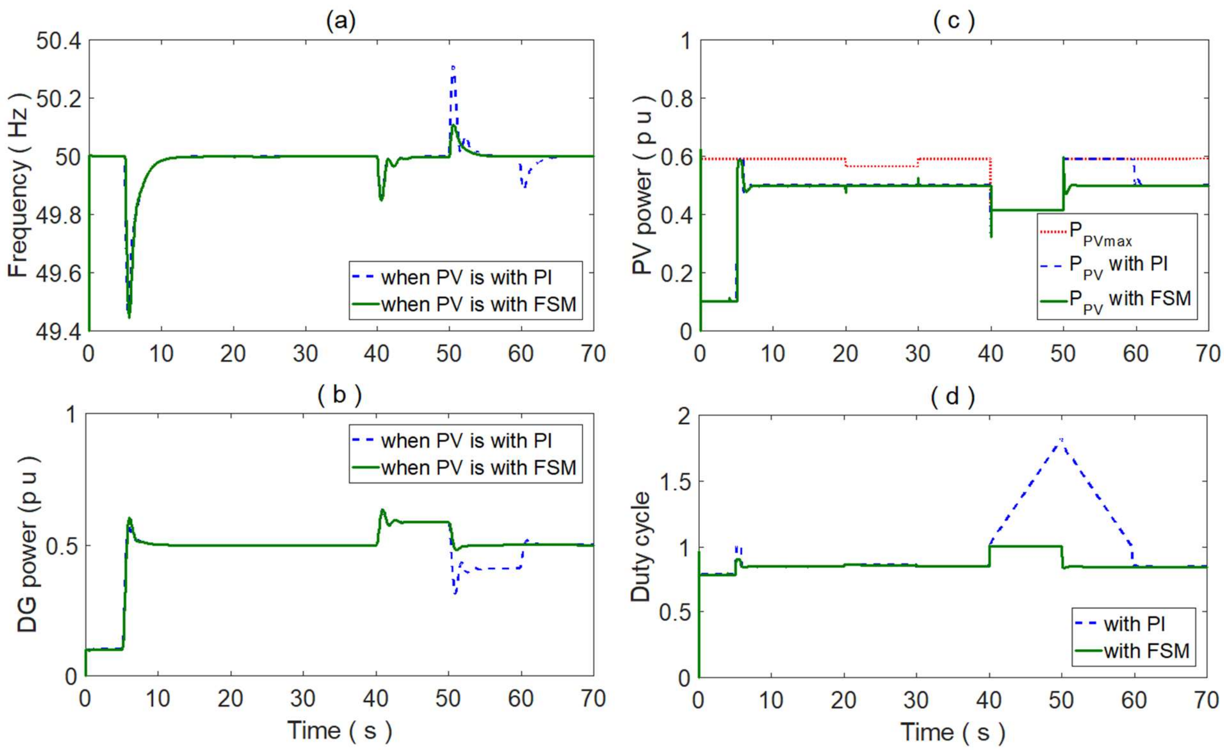

Figure 10. Responses of (a) frequency, (b) DG power, (c) PV power, (d) duty cycle during load variation and partial shading

From the results obtained in Fig.10, it can be concluded:

- When a load of 0.8 p.u. is applied at t = 5 s, the responses obtained with the PI control and the FSM control are similar.
- When a partial shading with a slight depth is applied at t= [20, 30 s] (the available PV power is greater than the requested power), there is a no change in the responses.
- When a partial shading with a deep depth is applied at t= [40, 50 s] (the available power is lower compared to the requested power), the FSM control remains stable (the value of the duty cycle is kept at 1) and the PI controller becomes unstable (increase in the value of the duty cycle), in contrast, the response of PV

power is maintained stable, due to the buck converter action which naturally limited the V_{pv} decrease.

- At t= [50, 60 s] (no partial shading), the system quickly returns to normal operation with FSM control, as compared to PI control which is much slower (the delay can last longer if the time of the partial shading is large).

From these results, it can be noted that during the partial shading, the buck converter was able to keep the system responses stable with the PI control. The FSM, on the other hand, was able to make the control stable, robust and fast.

7. Conclusion

This article proposes a new two-stage power converter topology for a Photovoltaic (PV) system without energy storage device and its control scheme based on a hybrid robust fuzzy sliding mode control (FSM). The aim is to enable the PV power system to support the grid inertia and contribute to frequency regulation.

Unlike other research, where the dc-dc boost converter has been widely used in PV systems, our work has proposed to use the dc-dc buck converter instead. The advantage of using the buck converter is the simplified design of the control law, which allows the PV power system to operate in the right side of their characteristic and hence will have the capacity to deliver power from almost zero to the maximum power.

Furthermore, the use of the FSM control provides additional robustness to the control scheme under variable whether conditions such as temperature, solar irradiance, and partial shading.

The proposed strategy has been validated via a series of real time simulations using OPAL-RT system under different power constraints and different grid frequency regulation schemes. The results obtained confirm the effectiveness, speed of response and accuracy of the proposed solution.

Appendix 1: Grid Code Technical Issues on Real Power Management

Different grid codes to connect PV plants to the grid and provide for real power controls are shown in Fig. 11.

A. Absolute power constraint

In using such control mode, the real power produced must not exceed a maximum level predefined by the grid operator, even in the case of power excess. Below the maximum level, the PV system is controlled to provide its available power. The main reason for using this control mode is to avoid generating more power than what is required by the load. Otherwise, the excess of power will have to be exported to neighboring power grids at no charge. This is illustrated in Fig.11.a.

B. Delta production constraint

The Delta mode of control is used to limit the generation below the available power with a fixed power reserve (ΔP) as depicted in Fig. 11.b. This control allows PV energy to participate in the primary frequency regulation. If the latter decreases, the source will be able to increase its output while keeping the frequency within acceptable range. In addition, this control can help reduce fluctuations in real power.

C. Power gradient constraint

Here the power variation is limited to a certain speed kW/s. This constraint is used to prevent rapid changes in real power from affecting grid stability. To achieve its functionality, the PV farm should be equipped with an accurate tool for predicting very short-term solar irradiation and temperature in the order of 10 sec. This control mode is illustrated in Fig.11.c.

D. Balance control

During the balance control mode, the PV power plant must be able to increase or decrease its delivered power very quickly to support the electrical grid in balancing supply and demand of real power as shown in Fig. 11.d. The PV power plant then participates in the secondary frequency regulation and must be interfaced with the grid operator's dispatching station.

E. System protection

The system protection control type is used to protect the electricity grid when there is an excess of generation. In such a type of control, the PV power plant must quickly reduce its power output. The value of the PV power is predefined and updated by the grid operator. The reduction will be maintained until the issued command signal to trigger the protection is disabled. The approach is illustrated in Fig.11.e.

458 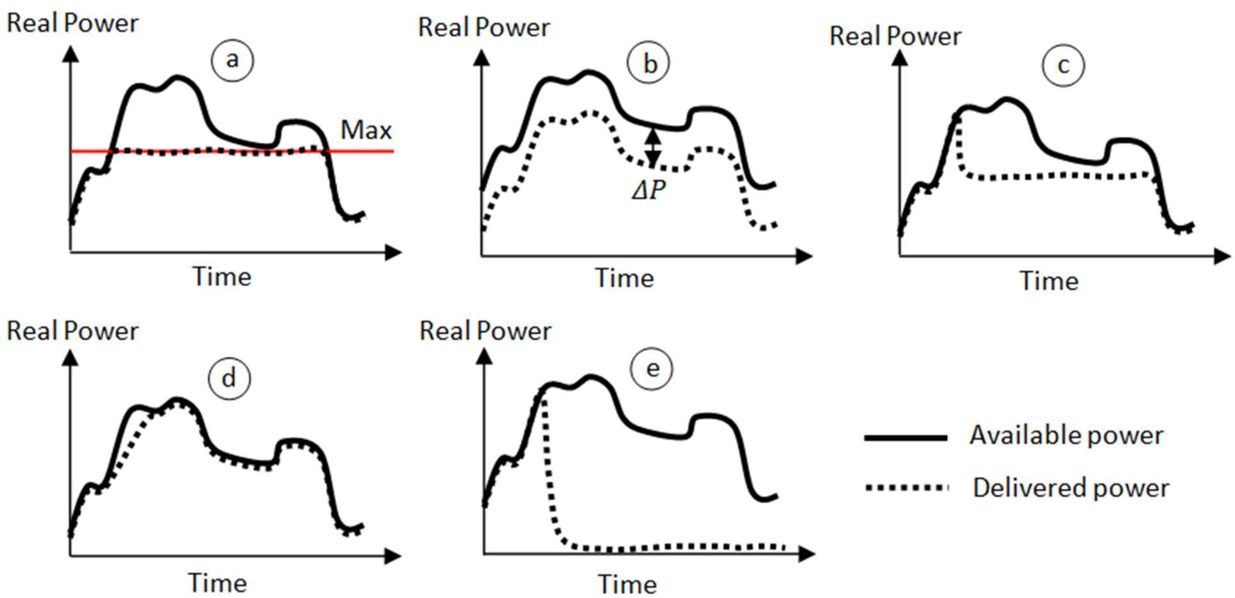

459 Figure 11. Constraints on real power management capabilities: (a) absolute
460 power constraint, (b) delta power constraint, (c) power gradient constraint, (d) balance
461 control, (e) system protection [26]

462
463 **Appendix 2 Control of the dc/ac converter**
464

465 The objective of the dc/ac converter is to: (i) keep the DC bus voltage constant
466 regardless of the PVG power magnitude (optimal transfer of power to the electrical grid)
467 and (ii) ensure independent control of real and reactive powers between the DC bus and
468 the grid with a unity power factor. Fig.12 shows the block diagram of the DC-AC
469 converter control.

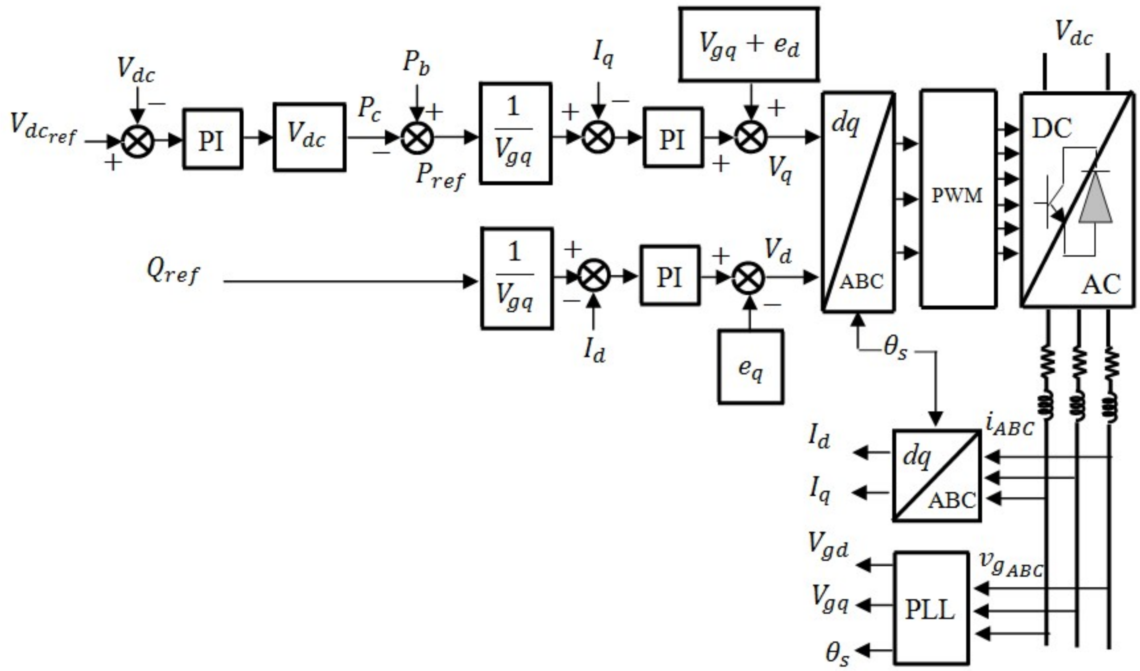

Figure 12. DC-AC converter control

A. Independent control of real and reactive power

The converter is connected to the grid through a three-phase filter. Thus, the voltages of phase A, B and C at the terminals of the filter are written:

$$\begin{cases} v_A = -R_f i_A - L_f \dfrac{di_A}{dt} + v_{gA} \\ v_B = -R_f i_B - L_f \dfrac{di_B}{dt} + v_{gB} \\ v_C = -R_f i_C - L_f \dfrac{di_C}{dt} + v_{gC} \end{cases} \quad (16)$$

Applying Park's transformation to this three-phase voltage, gives:

$$\begin{cases} V_d = -R_f I_d - L_f \dfrac{dI_d}{dt} + \omega_s L_f I_q + V_{gd} \\ V_q = -R_f I_q - L_f \dfrac{dI_q}{dt} + \omega_s L_f I_d + V_{gq} \end{cases} \quad (17)$$

The real and reactive powers generated by the converter are defined by:

$$\begin{cases} P = V_{gd}.I_d + V_{gq}.I_q \\ Q = V_{gq}.I_d - V_{gd}.I_q \end{cases} \tag{18}$$

By choosing the rotating field as reference frame $d-q$ reference frame ($V_{gd} = 0$), Eq. (17) becomes:

$$\begin{cases} V_d = -R_f I_d - L_f \dfrac{dI_d}{dt} + e_d \\ V_q = -R_f I_q - L_f \dfrac{dI_q}{dt} + e_q + V_{gq} \end{cases} \tag{19}$$

Where the coupling terms between the two axes d and q are written as:

$$\begin{cases} e_d = \omega_s L_f I_q \\ e_q = \omega_s L_f I_d \end{cases} \tag{20}$$

Taking into account the orientation of the reference $d-q$ related to the rotating field, Eq. (18) becomes:

$$\begin{cases} P = V_{gq} I_q \\ Q = V_{gq} I_d \end{cases} \tag{21}$$

Thus, the real and reactive powers are controlled by I_q and I_d respectively.

The model of the converter connected to the grid expressed in the rotating field reference frame given by Eq. (19) shows that we can set up a controller for each current component flowing in the filter. The reference quantities for these controllers will be the filter currents in the $d-q$ axes.

B. DC bus voltage control

By neglecting the harmonics due to switching and all losses in the converter and filter, the powers of the DC bus are:

$$\begin{cases} P = V_{dc}I \\ P_b = V_{dc}I_b \\ P_c = V_{dc}I_c \end{cases} \tag{22}$$

Where P is the real power flowing through the dc-ac converter, P_b is the output power of the buck converter, and P_c is the power required to charge the capacitor C_{dc}.

These powers are related by the following equation:

$$P = P_b - P_c \tag{23}$$

By controlling the power P, the power P_c in the capacitor can then be controlled and subsequently the voltage of the DC bus can be controlled. Therefore, the powers P_b and P_c must be known to determine P_{ref}.

The reference power for the capacitor is related to the reference current flowing in the capacitor as follows:

$$P_{c_{ref}} = V_{dc}I_{c_{ref}} \tag{24}$$

The DC bus voltage is then controlled by an external loop (with respect to the internal current regulation loop), with a controller generating the reference current $I_{c_{ref}}$ in the capacitor.

C. Determination of the PI controller parameters

The control of the converter involves three controllers, two for controlling the filter currents and one controller for the DC bus voltage. To design the control loops, it is assumed that the converter is ideal, and the coupling terms are neglected. It can be noticed that the transfer functions of the two currents are identical therefore the two controllers will have the same parameters.

The block diagram of the closed-loop current control I_q is shown in Fig.13.a.

The PI controller parameters are calculated so that the closed-loop transfer function is first order.

$$\begin{cases} K_p^{I_q} = \dfrac{3L_f}{t_s^{I_q}} \\ K_i^{I_q} = \dfrac{3R_f}{t_s^{I_q}} \end{cases} \tag{25}$$

The block diagram of the closed-loop DC bus voltage control is shown in Fig.13.b.

The PI controller parameters are calculated so that the closed-loop transfer function is second order with damping ξ and natural frequency ω_0.

$$\begin{cases} K_p^{V_{dc}} = 2\xi C_{dc}\omega_0 \\ K_i^{V_{dc}} = C_{dc}\omega_0^2 \end{cases} \tag{26}$$

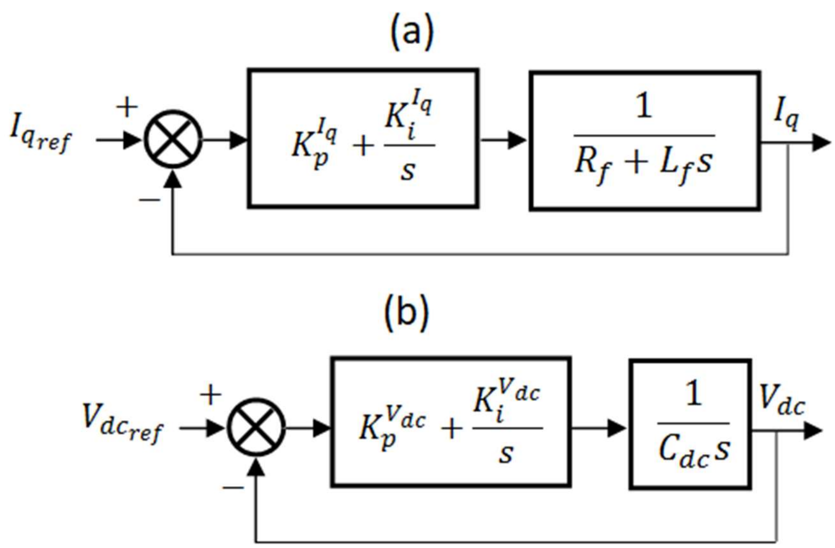

Figure 13. Control loop: (a) current component I_q, (b) DC bus voltage

NOMENCLATURE

C	Capacitance, F
C_{dc}	DC bus capacitance, F
e	Elementary charge on an electron, C
f	Grid frequency, Hz
H	Grid inertia constant, sec
I_{sat}	Diode saturation current, A
K	Boltzman constant, J/°K
L_{bf}	Buck filter inductance, H
L_f	Grid filter inductance, H
N_s	PV array series number
N_p	PV array parallel number
n	Quality factor
P_{pv}	PV system capacity, W
R_s	Series resistance, Ω
R_p	Parallel resistance, Ω
R	Resistance, Ω
R_{bf}	Buck filter resistance, Ω
R_f	Grid filter resistance, Ω
t_s	Settling time, sec

v_g	Grid voltage, V
V_{oc}	Open circuit voltage in standard condition, V
V_t	Thermal voltage, V

Greek Letters

θ_s	Position angle, rad
ω_s	Synchronous speed, rad/sec
ω_0	Cut-off frequency, rad/sec

REFERENCES

[1] Kumar Sahu B., 2015, "A study on global solar PV energy developments and policies with special focus on the top ten solar PV power producing countries," Renew Sustain Energy Rev, 43(March 2015), pp.621–634. https://doi.org/10.1016/j.rser.2014.11.058.

[2] IRENA, 2022, "Renewable Energy Statistics 2022," The International Renewable Energy Agency, Abu Dhabi, Report No. 978-92-9260-428-8. https://irena.org/publications/2022/Apr/Renewable-Capacity-Statistics-2022.

[3] Colmenar-Santos A, Linares-Mena AR, Molina-Ibáñez EL, Rosales-Asensio E, Borge-Diez D., 2020, "Technical challenges for the optimum penetration of grid-connected photovoltaic systems: Spain as a case study," Renew Energy, 145(January 2020), pp.2296–2305. https://doi.org/10.1016/j.renene.2019.07.118.

[4] Tielens P, Van Hertem D., 2016, "The relevance of inertia in power systems," Renew Sustain Energy Rev, 55(March 2016), pp.999–1009. https://doi.org/10.1016/j.rser.2015.11.016.

[5] Al-Shetwi AQ, Hannan MA, Jern KP, Mansur M, Mahlia TMI., 2020, "Grid-connected renewable energy sources: Review of the recent integration requirements and control methods," J Clean Prod, 253(April 2020), pp.119831. https://doi.org/10.1016/j.jclepro.2019.119831.

[6] Energinet, 2016, "Technical regulation 3.2.2 for PV power plants above 11 kW," energinet, danemark, Report No. 14/17997-32. www.energinet.dk.

[7] Liu J, Chen X, Cao S, Yang H., 2019, "Overview on hybrid solar photovoltaic-electrical energy storage technologies for power supply to buildings," Energy Convers Manag, 187(May 2019), pp. 103–121. https://doi.org/10.1016/j.enconman.2019.02.080.

[8] Clyde L, Peter K, Sirajul Ch, Stephen H, Mahesh M, Vladimir Ch, Nick M, Christopher M, Vahan G., 2017, "Demonstration of Essential Reliability Services by a 300-MW Solar Photovoltaic Power Plant," National Renewable Energy Laboratory (NREL), Report No NREL/TP-5D00-67799. https://www.nrel.gov/docs/fy17osti/67799.pdf.

[9] Hoke AF, Shirazi M, Chakraborty S, Muljadi E, Maksimovic D., 2017, "Rapid Active Power Control of Photovoltaic Systems for Grid Frequency Support," IEEE J Emerg Sel Top Power Electron, 5(3), pp.1154–1163. https://doi.org/10.1109/JESTPE.2017.2669299.

[10] Matevosyan J, Sharma S, Huang S-H, Woodfin D, Ragsdale K, Moorty S, Wattles P, Li W., 2015, "Proposed future Ancillary Services in Electric Reliability Council of

Texas," IEEE Eindhoven PowerTech, Eindhoven, Netherlands, 29 June 2015 - 02 July 2015 pp. 1-6, doi: 10.1109/PTC.2015.7232743.

[11] Joseph PV., 2016, "Power supply improvement plans (PSIPs)", Hawaiian Electric Companies, Report No. 2014-0183.

[12] Varma RK, Akbari M., 2020 "Simultaneous Fast Frequency Control and Power Oscillation Damping by Utilizing PV Solar System as PV-STATCOM," IEEE Trans Sustain Energy, 11(1), pp.415–425. https://doi.org/10.1109/TSTE.2019.2892943.

[13] Kamran Z, Waqar U, Muhammad A-K, Zunaib A, Muhammad U-A, Nicholas Ch, Kim H-J,. 2018 "A comprehensive review on inverter topologies and control strategies for grid connected photovoltaic system," Renew Sustain Energy Rev, 94(October 2018), pp.1120–1141. https://doi.org/10.1016/j.rser.2018.06.053.

[14] Batzelis EI, Kampitsis GE, Papathanassiou SA., 2017 "Power Reserves Control for PV Systems With Real-Time MPP Estimation via Curve Fitting, " IEEE Trans Sustain Energy, 8(3), pp.1269–1280. https://doi.org/10.1109/TSTE.2017.2674693.

[15] P. Veena, V. Indragandhi, R. Jeyabharath, V. Subramaniyaswamy, 2014, "Review of grid integration schemes for renewable power generation system," Renew. Sustain. Energy Rev, 34(June 2014), pp.628–641. https://doi.org/10.1016/j.rser.2014.03.034.

[16] Kouro S, Leon JI, Vinnikov D, Franquelo LG., 2015, "Grid-connected photovoltaic systems: An overview of recent research and emerging PV converter technology," IEEE Ind Electron Mag, 9(1), pp.47–61. https://doi.org/10.1109/MIE.2014.2376976.

[17] S. I. Nanou, A. G. Papakonstantinou, and S. A. Papathanassiou, 2015, "A generic model of two-stage grid-connected PV systems with primary frequency response and inertia emulation," Elect. Power Syst. Res., 127(October 2015), pp.186–196. https://doi.org/10.1016/j.epsr.2015.06.011.

[18] E. Batzelis, T. Sofianopoulos, and S. Papathanassiou, 2015, "Active power control in PV systems using a curve fitting algorithm based on the single-diode model," 31st European Photovoltaic Solar Energy Conference and Exhibition, Hamburg, Germany, 14-18 September, 2015, pp. 2402–2407. Doi:10.4229/EUPVSEC20152015-5BV.3.34.

[19] E. Batzelis, S. Nanou, S. Papathanassiou, 2014, "Active power control in PV systems based on a quadratic curve fitting algorithm for the MPP estimation," 29th European Photovoltaic Solar Energy Conference and Exhibition, Amsterdam, Netherlands, 23 - 25 September, 2014, pp. 3036–3040. Doi:10.4229/EUPVSEC20142014-5BV.3.13.

[20] E. I. Batzelis, S. A. Papathanassiou and B. C. Pal, 2018, "PV System Control to Provide Active Power Reserves Under Partial Shading Conditions," IEEE Transactions on Power Electronics, 33(11), pp. 9163-9175. doi: 10.1109/TPEL.2018.2823426.

[21] Nacar, M., Özer, E., and Yılmaz, A. E. (August 3, 2020). "A Six Parameter Single Diode Model for Photovoltaic Modules," ASME. J. Sol. Energy Eng, February 2021; 143(1): 011012. https://doi.org/10.1115/1.4047853.

[22] Moutis P, Vassilakis A, Sampani A, Hatziargyriou ND., 2015, "DC Switch Driven Active Power Output Control of Photovoltaic Inverters for the Provision of Frequency Regulation," IEEE Trans Sustain Energy, 6(4), pp.1485–1493. https://doi.org/10.1109/TSTE.2015.2450539.

[23] R. El Houda Thabet and H. Chafouk, 2016, "Set-membership methodology for multiple fault detection and isolation in DC-DC Buck Converters, " *18th Mediterranean Electrotechnical Conference (MELECON)*, Lemesos, Cyprus, 18-20 April, 2016, pp. 1-6. doi: 10.1109/MELCON.2016.7495377.

[24] Ardjoun, SAEM, Denai, M, Abid, M., 2019, "A robust power control strategy to enhance LVRT capability of grid-connected DFIG-based wind energy systems," Wind Energy, 22(6), pp.834– 847. https://doi.org/10.1002/we.2325.

[25] Kumar, N., and Sharma, A. (July 16, 2021). "Design and Analysis of Nonlinear Controller for a Standalone Photovoltaic System Using Lyapunov Stability Theory." ASME. J. Sol. Energy Eng. February 2022; 144(1): 011003. https://doi.org/10.1115/1.4051584

[26] de Alegría IM, Andreu J, Martín JL, Ibañez P, Villate JL, Camblong H., 2007, "Connection requirements for wind farms: A survey on technical requirements and regulation," Renew Sustain Energy Rev, 11(8), pp.1858–1872. https://doi.org/10.1016/j.rser.2006.01.008.

Figure Captions List

Fig. 1 Grid connected PV energy conversion system

Fig. 2 PVG I-V and P-V characteristics

Fig. 3 Classical control scheme of the buck converter: (a) general scheme, (b) I_{fb} current control block diagram

Fig. 4 Membership functions: (a) input variables $S(I_{fb})$, (b) output variables V_{fb}^{fuzzy}

Fig. 5 FSM control scheme of the buck converter

Fig. 6 Solar irradiance and temperature profiles used in the model

Fig. 7 Left panel: Responses in delta mode. Right panel: Responses in balance mode: (a) powers, (b) currents, (c) voltage

Fig. 8 Low inertia microgrid: (a) configuration (b) transfer function bloc diagram

Fig. 9 Partial shading profiles

Fig. 10 Responses of (a) frequency, (b) DG power, (c) PV power, (d) duty cycle during load variation and partial shading

Fig. 11 Constraints on real power management capabilities: (a) absolute power constraint, (b) delta power constraint, (c) power gradient constraint, (d) balance control, (e) system protection [26]

Fig. 12 DC-AC converter control

Fig. 13 Control loop: (a) current component I_q, (b) DC bus voltage

Table Caption List

Table 1 Fuzzy rules

Table 2 PV system parameter values

Table 3 Microgrid parameter values